Available online at www.sciencedirect.com
ScienceDirect
Journal of the European Ceramic Society 28 (2008) 1979–1986
www.elsevier.com/locate/jeurceramsoc

Failure of the plasma-sprayed coating of lanthanum hexaluminate

X.Q. Cao [a,*], Y.F. Zhang [a,b], J.F. Zhang [a,b], X.H. Zhong [a,b], Y. Wang [a], H.M. Ma [a], Z.H. Xu [a,b,c], L.M. He [c], F. Lu [c]

[a] *CAS Key Laboratory of Rare Earths on Advanced Materials and Valuable Utilization of Resources, Changchun Institute of Applied Chemistry, Chinese Academy of Sciences, Changchun 130022, Jilin, China*
[b] *Graduate School of the Chinese Academy of Sciences, Beijing 100049, China*
[c] *Beijing Institute of Aeronautical Materials, Beijing 100095, China*

Received 10 October 2007; received in revised form 17 January 2008; accepted 19 January 2008
Available online 10 March 2008

Abstract

Lanthanum magnesium hexaluminate ($LaMgAl_{11}O_{19}$, LMA) is an attractive material for thermal barrier coatings (TBCs), and the failure of its coating was studied in this work by thermal cycling, X-ray diffraction, dilatometric measurement and thermal gravimetric-differential thermal analysis. The dilatometric measurement indicates that even though the bulk material of LMA has a higher sintering-resistance than the typical TBC material, i.e. yttria-stabilized zirconia (YSZ), the plasma sprayed coating of LMA has two serious contractions due to the re-crystallization of LMA and phase transitions of alumina. LMA has similar thermal expansion behaviour with alumina, leading to a good thermal expansion match between LMA and the thermally grown oxide layer. On the other hand, the plate-like structure of LMA not only results in a low thermal conductivity, low Young's modulus, but also a high stress tolerance, and these are believed to be the reasons for the long thermal cycling life of LMA coating.

Keywords: Lanthanum magnesium hexaluminate; Plasma spraying; Phase stability; Thermal barrier coatings

1. Introduction

TBCs find an increasing number of applications to protect high-temperature metallic components. TBCs are deposited on transition pieces, combustion lines, first-stage blades and vanes, and other hot-path components of gas turbines either to increase the inlet temperature with a consequent improvement of the thermal efficiency or to reduce the requirements for the cooling system.[1] The selection of TBC materials is restricted by some basic requirements, including high melting point, phase stability between room temperature and operation temperature, low thermal conductivity, chemical inertness, thermal expansion match with the metallic substrate, good adherence to the metallic substrate, and low sintering rate of the porous microstructure.[1,2]

No single material satisfies all these criteria. The best compromise among these requirements is presently offered by the partially stabilized zirconia containing 7–8 wt% Y_2O_3 (i.e. 4.0–4.6 mol% Y_2O_3) on a MCrAlY bond coat, deposited either by plasma spraying or by electron beam-physical vapour deposition (EB-PVD).[1] A major disadvantage of yttria-stabilized zirconia (YSZ) is the limited operation temperature of 1200 °C for long-term application. At higher temperatures, phase transformations from the t'-tetragonal to tetragonal and cubic ($t+c$) and then to monoclinic (m) occur, giving rise to the coating failure.[2,3] The search for new materials that can withstand higher gas-inlet temperatures was intensified within the last decade. $La_2Zr_2O_7$ has been proposed as a candidate of TBC material.[2,4–6] It has a cubic pyrochlore structure which has been discussed in detail by Subramanian et al.[7] Compared with YSZ, it has a lower thermal conductivity (1.56 $W\,m^{-1}\,K^{-1}$ for $La_2Zr_2O_7$, 2.1–2.2 $W\,m^{-1}\,K^{-1}$ for YSZ, bulk materials, 1000 °C), lower thermal expansion coefficient ((9.1–9.7) $\times 10^{-6}\,K^{-1}$ for $La_2Zr_2O_7$, (10.5–11.5) $\times 10^{-6}\,K^{-1}$ for YSZ, bulk materials and coatings, 30–1000 °C) and lower sintering ability. However, its single layer coating has a very short life due to its low thermal expansion coefficient and low fracture toughness,[8] and the life could be improved if a double ceramic-layer coating of $La_2Zr_2O_7$ with 8YSZ was applied, especially for the high temperature application.[9,10]

* Corresponding author. Tel.: +86 431 85262285; fax: +86 431 85262285.
E-mail address: xcao@ciac.jl.cn (X.Q. Cao).

0955-2219/$ – see front matter © 2008 Elsevier Ltd. All rights reserved.
doi:10.1016/j.jeurceramsoc.2008.01.023

Lanthanum magnesium hexaluminate (LMA) is an important ceramic material for high temperature applications such as active elements of solid-state lasers,[11] combustion catalyst and catalyst support,[12,13] and TBC material.[14–18] It possesses long term structural and thermochemical stabilities up to 1400 °C, and has significantly lower sintering rate than the zirconia-based material. The low thermal conductivity of LMA is caused by its microstructure, i.e. a random arrangement of LMA platelets that build up a microporous coating and the insulating properties of the material with its crystallographic feature itself. A study describing the development of an optimized procedure for the processing, manufacturing and application of LMA as TBC material has been reported by Gadow.[16]

It is generally accepted that thermal expansion mismatches between the top ceramic coat and metallic bond coat and TGO are the strongest factors for coating failure.[19,20] TGO is composed of mainly alumina (Al_2O_3), some chromia (Cr_2O_3) and spinel ($NiAl_2O_4$). At the early stage of thermal cycling, the top ceramic coat contacts directly with the bond coat, and the thermal expansion mismatch plays the most important role in determining the thermal cycling life of TBCs. When the bond coat is oxidized and the TGO thickness reaches a critical value (8–10 μm for 8YSZ TBC[21]), the swelling of TGO would lead to the coating failure.

Gadow and co-workers have reported the basic thermomechanical properties of LMA and the preparation of its coating by plasma spraying.[14–18] In this work, the thermal stability and failure of LMA coating were studied.

2. Experimental

Main chemicals used in this work were La_2O_3 (99.99%, Guangdong Chenghai Sanxing Chemicals Co., Ltd.), MgO (99.2%, Wuxi Zehui Chemicals Co., Ltd.) and γ-Al_2O_3 (99.99%, Tangshan Haigang Huatai Functional Ceramic Materials Co., Ltd.). The starting powder for the plasma-sprayed LMA coating was synthesized by solid-state reaction. The powder mixture of La_2O_3, MgO and γ-Al_2O_3 in proper ratio was heated at 1600 °C for 6 h. The as-synthesized LMA powder was mixed with water and Gum Arabic, followed by ball-milling with zirconia balls (Tosoh). When the grain size of LMA in the slurry was smaller than 1 μm, the slurry was spray-dried (GZ-5, Yangguang Ganzao). The free-flowing powder with particle size between 20 and 100 μm was collected and used directly for plasma spraying without other treatments.

The plasma-sprayed coatings were produced by atmospheric spraying with a Praxair-Tafa 5500-2000 Plasma Spray unit with Ar–H_2 as plasma gas. Before the plasma spraying, the substrate was heated to 300–400 °C with the plasma flame. LMA coating (thickness ~300 μm, Ø30 mm) for burner-rig test was made by plasma spraying on a superalloy substrate with a MCrAlY (M=Ni, Co, Fe) bond coat. The disk-shaped substrate had a thickness of 3 mm and a bevelled edge to minimize the effect of stresses originated at the free edge of the specimens. The test was carried out with a coal gas flame whose temperature was higher than 1700 °C. The sample surface was cycled from room temperature to 1250 °C (bond-coat temperature 970 °C) for 5 min followed by quenching to room temperature within 2 min by a compressed air jet, each cycle lasted 7 min. The surface temperature was monitored with a long wavelength infrared-radiation pyrometer KT1599II (Heitronics, spectral range 9.6–11.5 μm) whose emissivity was set to be 0.86,[22] and the bond-coat temperature was measured with a standard Pt/Pt–Rh_{10} thermal couple. The powder for 8YSZ coating was 204NS from Sulzer Metco.

The coating microstructure was studied by scanning electron microscope (SEM, XL-30 ESEM FEG, Micro FEI Philips). The thermogravimetric-differential thermal analyses (TG-DTA) of LMA coating were performed simultaneously on a thermoanalyzer (TA SDT 2960) in air atmosphere with a heating rate of 10 °C min^{-1}. The dilatometric measurement of LMA coating was carried out with a high-temperature dilatometer (Netzsch 402C). During the dilatometric measurement, a small piece of coating (1.3 mm × 5 mm × 25 mm) was heated from 35 to 1400 °C with a heating rate of 5 °C min^{-1} and then held for 10 h followed by cooling down to room temperature. The coating for the dilatometric and Young's modulus measurements was prepared by plasma spraying of LMA powder on a graphite substrate, followed by cutting and heating up to 700 °C for 1 h to burn off graphite. The sample for TG-DTA was prepared by abrading the graphite substrate without any heat treatment. The sample dimension for Young's modulus measurement (Instron Model 1121) was 1.3 mm × 5 mm × 35 mm.

In order to study the chemical stability of LMA against TGO at a temperature when the coating was used, a mixture of Al_2O_3 and LMA in a molar ratio of 50:50 was ball-milled with a high-energy milling machine until the grain size was smaller than 1 μm. The mixture was then heated at 1300 °C for 24 h, and X-ray diffraction (XRD, Rigaku D/Max-IIB Diffractometer, Cu Kα radiation) was applied to analyze the final product. Coatings without polishing were used directly for XRD measurement.

Fourier transmission infrared spectra (400–4000 cm^{-1}, Bruker Vertex 70 FTIR) of LMA powder and its coatings were measured with KBr as the solid solvent. Before the measurement, LMA coatings were crashed into fine powders and dried at 110 °C for 1 h under vacuum.

3. Results and discussion

3.1. Failure of LMA coating

Gadow and co-workers have reported the synthesis of LMA by means of sol–gel.[16–18] In this work, a solid-state method was applied to synthesize LMA on a large scale, which is more convenient than sol–gel. After being heated at 1600 °C for 6 h, the formation of LMA was completed, and the plate-like structure was observable as shown in Fig. 1. The platelet looks very dense and has a thickness of 1–2 μm. The plate-like structure is believed to be the reason for its low thermal conductivity.[16]

One LMA coating was tested with a gas burner facility for 11,970 cycles, corresponding to a total heating time of 998 h. A small spallation was observed at the coating edge after about 11,000 cycles, and after 11,970 cycles a large piece of coating peeled off as shown in Fig. 2. The thermal cycling life of LMA coating is close to that of the typical coating material 8YSZ

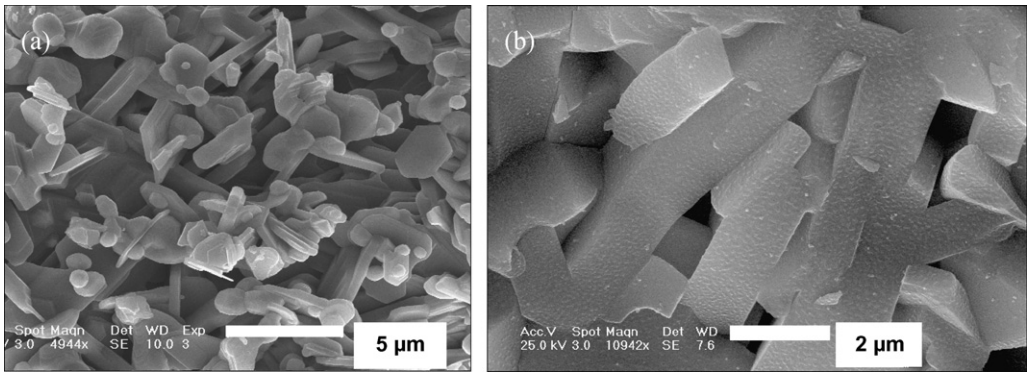

Fig. 1. Morphology of LMA powder calcined at 1600 °C for 6 h with low magnification (a) and 1650 °C for 6 h with large magnification (b).

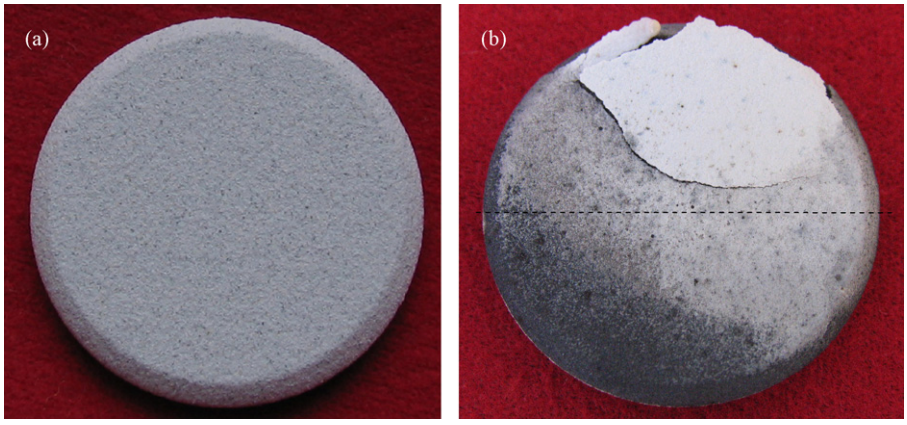

Fig. 2. LMA coating before (a) and after (b) thermal cycling. The dashed line of (b) shows the cutting direction of the coating for microstructure analysis by SEM.

under a similar test condition. The black spots on the coating surface (see the bottom and left side of Fig. 2b) are induced by the contamination of metallic oxides from the sample holder of the test facility.

The microstructure of LMA coating surface after thermal cycling is shown in Fig. 3. The surface looks porous, and the platelets whose thicknesses are between 50 and 80 nm are clearly shown in Fig. 3c, the thickness is much smaller than that of the calcined powder as shown in Fig. 1b. The temperature of plasma flame is about 15,000 °C. During plasma spraying, the powder is instantly molten and cooled immediately when the molten droplet leaves the flame, and the cooling rate is estimated to be higher than 10^6 K s^{-1}.[23] The thin platelet of LMA coating is an indication of nonperfect crystallization during plasma spraying.

The cross-sectional microstructures of LMA coating after thermal cycling are shown in Fig. 4. The coating cracked mainly at the interface between the coating and bond coat, and the large vertical crack could also be observed at the bevelled edge under a large magnification as shown in Fig. 4a. The coating at the bevelled edge is in the state of tensile stress, and this is usually the place where the failure begins. The microstructures in detail of LMA coatings before and after thermal cycling are compared in Fig. 5. Before thermal cycling as shown in Fig. 5a, the coating shows a porous and typical structure of the plasma sprayed coatings, and the thickness is about 330 μm. The binding of LMA coating to bond coat looks perfect, showing a good melting condition of LMA powder in the plasma flame. After thermal cycling as shown in Fig. 5b, the coating thickness is slightly reduced to

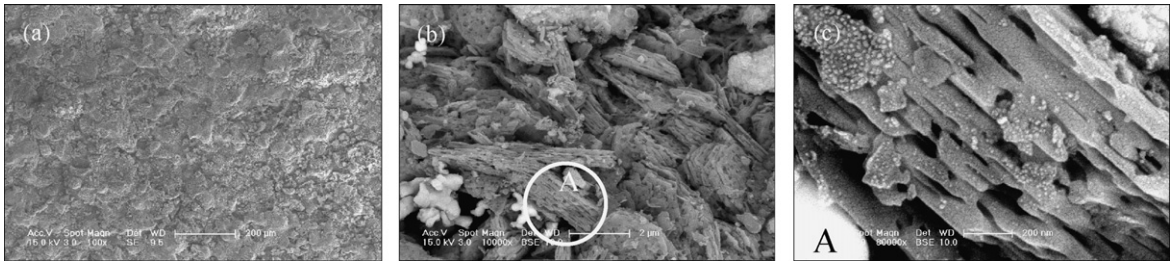

Fig. 3. SEM micrographs of LMA coating surface after thermal cycling with different magnifications: (a) $10^2\times$; (b) $10^4\times$; (c) $(8\times10^4)\times$, the selected location A of (b).

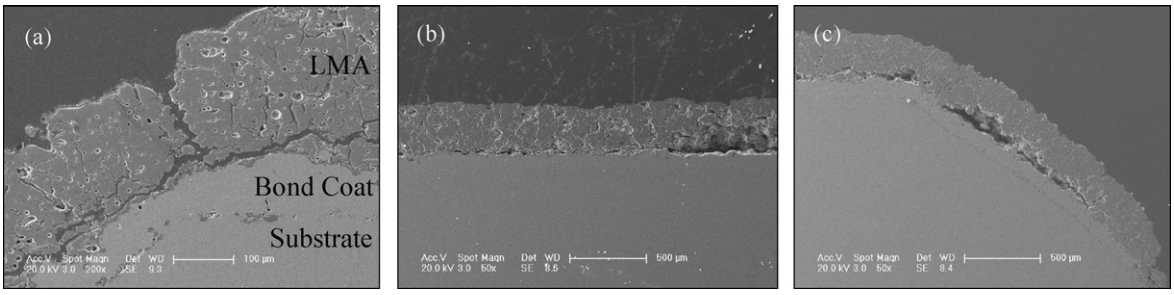

Fig. 4. SEM micrographs of the cross-section of LMA coating after thermal cycling: left edge of the coating with a magnification of 200× (a), central part (b) and right edge (c) with a magnification of 50×.

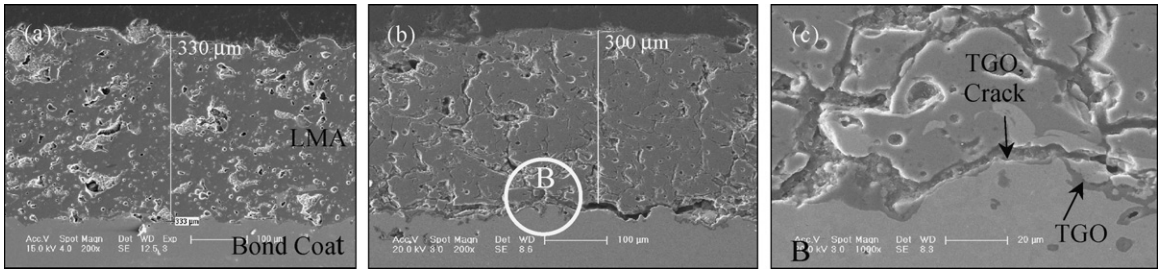

Fig. 5. SEM micrographs of the cross-section of LMA coating center before (a) and after (b) thermal cycling. (c) The selected location B of (b) with large magnification.

300 μm, and the coating looks a little bit denser than that before thermal cycling. The microstructure of the interface between bond coat and LMA coating is clearly shown in Fig. 5c. It is interesting that TGO is not so obvious as normally observed in YSZ coating, and the crack mainly occurs at TGO which is similar to the failure mode of the coating made by EB-PVD.[24] It is well-known that the spallation of the plasma-sprayed YSZ coating usually occurs at the YSZ side which is a few microns away from and parallel to TGO layer,[25] and therefore TGO is still perfect even after the spallation.

The elemental distribution at the interface of LMA coating and bond coat was analyzed by means of EDS (energy dispersive spectroscopy), and the results are shown in Fig. 6. As expected, TGO is rich in O and Al. The high contents of O and Al extend to a distance of approximately 20 μm from TGO towards bond coat (see the left side of the black square in Fig. 6b), implying that bond coat has been deeply oxidized during the long-time thermal cycling. On the other hand, on the right side of TGO (see the right side of the black square in Fig. 6b), the high content of Y extends to a distance of approximately 10 μm towards LMA coating, but this location is poor in La and Mg. It seems that a thin layer of oxides containing mainly O, Y, Al and some La and Mg was formed between TGO and LMA during thermal cycling. The formation of this oxide layer must be a result of selective oxidation of alloying elements in bond coat whose main composition is MCrAlY (M=Ni, Fe, Co). It seems that Y diffuses out and "penetrates" TGO layer during thermal cycling. Both Y and La belong to the rare earth group, and they have very similar properties and ionic radii, therefore, it would be easy for La in LMA to be substituted by Y when Y diffuses out and reaches the LMA side. It has also been observed in Toscano's work that the Y incorporation into TGO is also an important lifetime governing factor of TBC which results in an increase of the TGO growth rate and in parallel in a decrease of the Y content in the YSZ

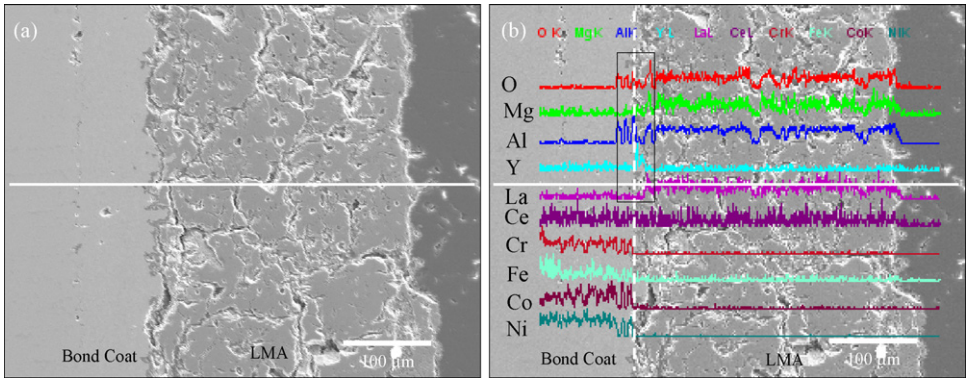

Fig. 6. SEM micrograph of the cross-section (a) and the corresponding elemental analysis by EDS (b) for LMA coating which is still perfect without serious spallation after thermal cycling. The black square highlights the location where O, Mg, Al, Y and La are concentrated; the white dashed line shows the border between bond coat and LMA.

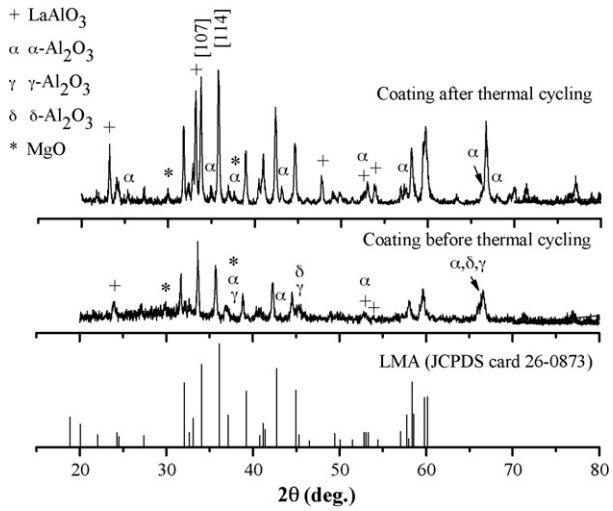

Fig. 7. Comparison of XRD patterns of LMA coating before and after thermal cycling.

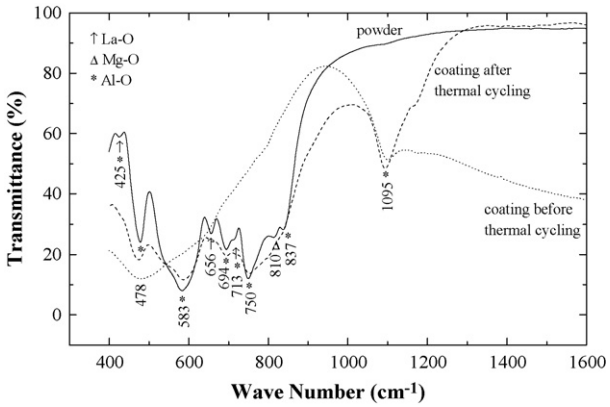

Fig. 8. FTIR spectra of LMA powder and its coatings.

coating.[26] If the Y concentration is reduced beneath a critical level, its positive effect on TGO adherence is lost, resulting in TGO spallation.

The plasma sprayed coatings of LMA and 8YSZ which were prepared under the same coating parameters were tested with Instron Model 1121 for the measurement of Young's modulus. The porosities of these two coatings are between 10% and 20% as measured by Archimedean method. LMA coating has a slightly lower Young's modulus (8.65 GPa) than 8YSZ coating (8.91 GPa) as expected.

3.2. Phase stability of LMA coating

The XRD patterns of LMA coating surface before and after thermal cycling are compared in Fig. 7. Except for a few weak peaks as marked in the pattern, the plasma sprayed coating before thermal cycling shows the typical pattern of LMA, but its intensity is low, indicating that crystallization is not perfect owing to the fast cooling rate plasma spraying. After thermal cycling, the re-crystallization is finished, and the peaks are highly intensified. On the other hand, a lot of weak peaks are observed before thermal cycling, they are intensified after thermal cycling, and these peaks are correlated to $LaAlO_3$, MgO and α,δ,γ-Al_2O_3. As reported in our former work,[27] with La_2O_3, MgO and Al_2O_3 as the starting materials, the intermediate product was $LaAlO_3$ below 1400 °C, the formation of LMA was finished above 1500 °C and pure LMA could be obtained at 1600 °C for 6 h. The existences of $LaAlO_3$, MgO and α,δ,γ-Al_2O_3 in the coating indicate that LMA was partially decomposed during plasma spraying due to the extremely high temperature of plasma flame. During thermal cycling of the coating, the temperature of coating surface was below 1300 °C which was much lower than the formation temperature of LMA, therefore, these decomposition products still existed in the coating even though the coating was thermally cycled. On the other hand, the peak [107] is the strongest before thermal cycling and the peak [114] becomes the strongest after thermal cycling, implying that the crystal direction [107] is the most favoured during the fast crystallization. Fig. 7 also shows that δ,γ-Al_2O_3 has transformed to α-Al_2O_3 during thermal cycling. The plasma-sprayed coating of alumina usually contains mainly γ-Al_2O_3 and some α,δ-Al_2O_3, the phase transitions of $\gamma \rightarrow \delta$ and $\delta \rightarrow \alpha$ occur at 1000 °C and 1100 °C, respectively.[28–30] The phase transition of $\gamma \rightarrow \delta$ is companied by a volume expansion,[28] and the net shrinkage of the process $\gamma \rightarrow \alpha$ is about 2%.[29] Both coatings of silica and alumina have re-crystallization or phase transition above 1000 °C. The re-crystallization or phase transition would make serious contractions and cracks for their coatings, and this is the main reason that they can not be used as TBC materials for the applications above 1000 °C.[31] Even though LMA coating has re-crystallization and phase transition above 900 °C, but it still has a long thermal cycling life, indicating that LMA has a high stress tolerance due to the platelet structure.

FTIR spectra in the range of 400–1600 cm^{-1} are shown in Fig. 8. In the range of 1600–4000 cm^{-1}, no absorption peaks were detected except those of CO_2 and H_2O, and the results in this range are not shown here. By comparing the standard spectra of La_2O_3, MgO and Al_2O_3, the absorption peaks of LMA powder are indexed as shown in Fig. 8. Those peaks are strong and sharp. However, the absorption peaks of the coating before thermal cycling are weak and broadened, showing a character of nonperfect crystallization which is consistent with the XRD result above. After thermal cycling, the re-crystallization was finished and its spectrum is very similar to that of the powder. The coatings have a strong peak at 1095 cm^{-1} where it is very weak for the powder, this may be induced by the decomposition products of the coating, such as $LaAlO_3$ or Al_2O_3.

The dilatometric measurements of the plasma sprayed coatings of LMA and 8YSZ are compared in Fig. 9. For the bulk material of LMA which was prepared by solid state method, the averaged thermal expansion coefficient between room temperature and 1400 °C is $9.1 \times 10^{-6}\,K^{-1}$, this value is close to that of Gadow ($10.1 \times 10^{-6}\,K^{-1}$).[15] Below 885 °C, LMA coating expands with the increase of temperature, resulting in an averaged thermal expansion coefficient of $7.3 \times 10^{-6}\,K^{-1}$. However, LMA coating has two serious contractions in the temperature ranges of 885–1010 °C and 1134–1335 °C, respectively. Above 1335 °C and after being sintered at 1400 °C for

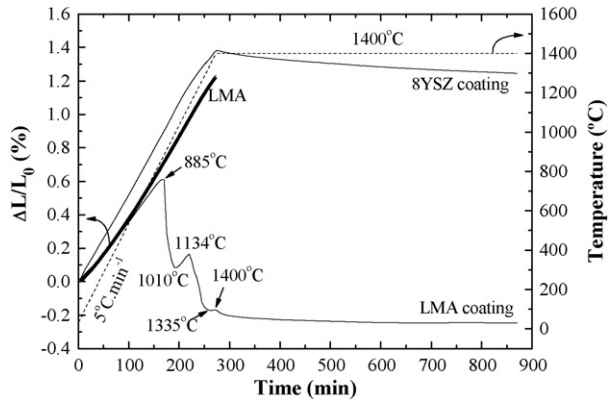

Fig. 9. Dilatometric measurements of LMA bulk material and the plasma sprayed coatings of LMA and 8YSZ.

10 h, the coating contracts for only 0.051% which is much lower than that of 8YSZ coating (0.137%). The net shrinkage of LMA coating after the dilatometric measurement is 0.25%.

In order to understand the reason for the thermal contraction, the thermal gravimetric-differential thermal analyses (TG-DTA) were carried out with a small piece of LMA coating and the result is shown in Fig. 10. The coating shows three steps of weight loss starting at 107, 410 and 524 °C, respectively, leading to a total weight loss of approximately 0.6%. The first loss could be attributed to the loss of the adsorbed moisture. The most possible reason for other two steps is the loss of OH species at elevated temperatures. In air atmosphere and at high temperature, the oxide ceramic reacts with H_2 and the formation of OH species in the plasma flame (Ar–H_2) is possible. Except for the alkaline metallic hydroxides, the decomposition of other hydroxides usually occurs below 700 °C. For example, the decomposition temperatures of OH species in $La(OH)_3$, $Mg(OH)_2$ and $Al(OH)_3$ are 350–580 °C,[32] 350 °C[33] and 300–420 °C,[33,34] respectively. The decomposition of carbonate-containing species occurs at some higher temperature, for example, 670–810 °C for $La_2(CO_3)_3$[32] and 350–900 °C for $Mg(OH)_2{\cdot}MgCO_3$.[33] OH species in the coating are not detected by FTIR because the content is not high enough. On the other hand, it is clear that the loss of OH species does not show influence on the dilatometric behaviour of the coating.

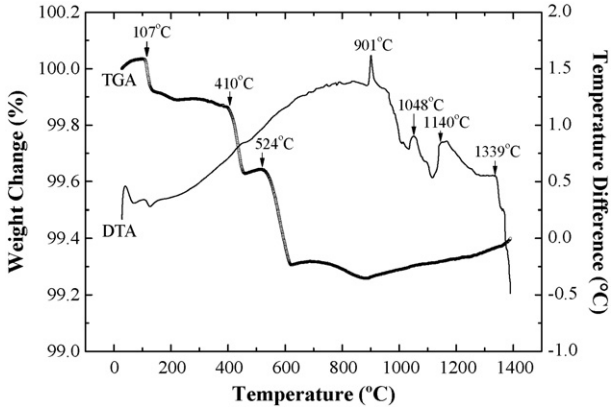

Fig. 10. TG-DTA curves of plasma sprayed LMA coating.

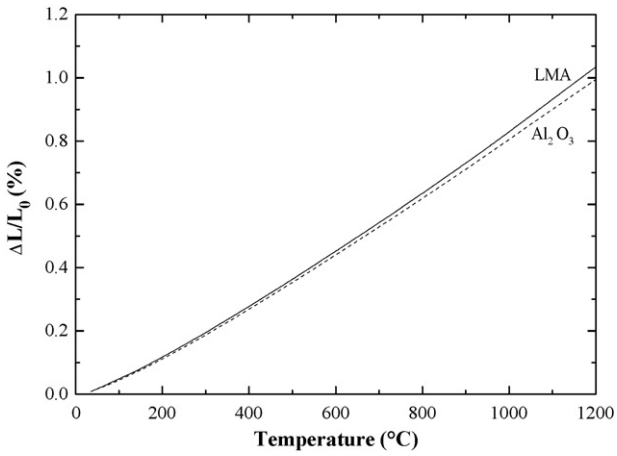

Fig. 11. Comparison of thermal expansion behaviours of LMA and Al_2O_3 bulk materials, both of them were densified at 1650 °C for 6 h.

In DTA curve, there are obviously three exothermic peaks at 901, 1048 and 1140 °C, respectively. The first and the third exothermic peak agree well with the two contractions (885–1010 °C, 1134–1335 °C) of the dilatometric curve as shown in Fig. 9. The second exothermic peak falls into the expansion process (1010–1134 °C). As observed by XRD (Fig. 7), the coating before thermal cycling consists of the nonperfectly crystallized LMA and metastable phases of alumina including γ,δ-Al_2O_3. The phase transitions of γ → δ and δ → α occur at 1000 and 1100 °C, respectively.[28–30] and the process of γ → δ is accompanied by a volume expansion.[28] Even though no strong evidences are supported here, it is suggested that the three exothermic peaks correspond to the recrystallization of LMA, the phase transitions of γ → δ-Al_2O_3 and δ → α-Al_2O_3, respectively. The phase transitions in LMA coating are complicated, high-resolution XRD is necessary to study these processes and this work is still in progress.

3.3. Comparison of LMA with Al_2O_3

LMA and Al_2O_3 have a lot of similarities, such as crystal structure (hcp), thermal expansion behaviour and composition, etc. The comparison of thermal expansion behaviours of LMA and Al_2O_3 bulk materials is shown in Fig. 11. These two materials have very similar thermal expansion behaviours. In the range of room temperature to 1200 °C, the averaged thermal expansion coefficients are $9.1 \times 10^{-6}\,K^{-1}$ for LMA ($7.3 \times 10^{-6}\,K^{-1}$ for its coating) and $8.6 \times 10^{-6}\,K^{-1}$ for Al_2O_3 ($8.0 \times 10^{-6}\,K^{-1}$ for its coating).[35] The similar thermal expansion behaviour is very helpful to the prolongation of thermal cycling life of LMA coating when the TGO layer is formed. Therefore, before the plasma spraying of LMA, the bond coat surface had been heated with the plasma flame to make a thin layer of TGO. Furthermore, the preheating of substrate could also effectively reduce the residual stress in the coating. For instance, before the deposition of LMA coating by air plasma spraying, the metallic substrate was preheated from 150 to 340 °C, and the as-deposited coating had the lowest stress.[16] High tensile stress is formed if the substrate is simultaneously cooled during deposition.

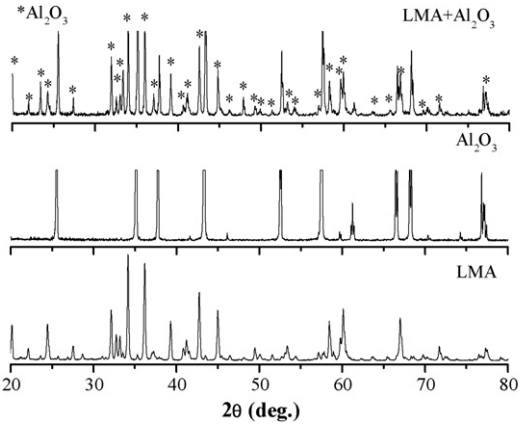

Fig. 12. XRD patterns of the mixture of LMA and Al_2O_3 after being heated at 1300 °C for 24 h.

In order to study the stability of LMA when it contacts TGO, a mixture of LMA and Al_2O_3 in a molar ratio of 50:50 was heated at 1300 °C for 24 h, and the XRD results are shown in Fig. 12. After the thermal treatment, the mixture still shows the typical XRD patterns of LMA and Al_2O_3 without the formation of any new phase, indicating that LMA and Al_2O_3 do not have solubility in each other. It could be concluded that LMA is stable at the application temperature of TBCs which is below 1300 °C.

4. Conclusion

The spallation of LMA coating occurs mainly at TGO which is similar to the coating made by EB-PVD. The similar thermal expansion behaviour of LMA with Al_2O_3 is very helpful to the prolongation of thermal cycling life of LMA coating, and therefore it is suggested to make a thin layer of TGO before the deposition of LMA. On the other hand, even though the plasma-sprayed LMA coating has phase transition during thermal cycling, the plate-like and porous structure of LMA results in a low Young's modulus and a high stress tolerance, and these are believed to the reasons for the long thermal cycling life of LMA coating.

Acknowledgement

The authors thank Ms. M.Y. Li for SEM analysis and Mr. G. Li for XRD measurement, Dr. Q.S. Wang of Beijing Polytechnic University for the invaluable assistance in plasma spraying. This work was financially supported by the project of A1320061002.

References

1. Cernuschi, F., Bianchi, P., Leoni, M. and Scardi, P., Thermal diffusivity/microstructure relationship in Y-PSZ thermal barrier coatings. *J. Therm. Spray Technol.*, 1999, **8**(1), 102–109.
2. Vassen, R., Tietz, F., Kerkhoff, G. and Stoever, D., New materials for advanced thermal barrier coatings. In *Proceedings of the 6th Liége Conference on Materials for Advanced Power Engineering*, ed. J. Lecomte-Beckers, F. Schuber and P. J. Ennis. Universite de Liége, Belgium, November 1998, ASM Thermal Spray Society, 1998, pp. 1627–1635.
3. Thornton, J. and Majumdar, A., Ceria precipitation and phase stability in zirconia based thermal barrier coatings. In *Proceedings of the International Thermal Spray Conference'95*, ed. A. Ohmori. Kobe, Japan, May 1995, ASM Thermal Spray Society, 1995, pp. 1075–1080.
4. Maloney, M. J., Thermal barrier coating systems and materials. European Patent EP 0848077 A1, 1998.
5. Vassen, R., Cao, X., Tietz, F., Kerkhoff, G. and Stoever, D., $La_2Zr_2O_7$—a new candidate for thermal barrier coatings. In *Proceedings of the United Thermal Spray Conference'99*, ed. E. Lugscheider and P. A. Kammer. Duesseldorf Germany, March 1999, ASM Thermal Spray Society, 1999, pp. 830–834.
6. Vassen, R., Cao, X., Tietz, F., Basu, D. and Stoever, D., Zirconates as new materials for thermal barrier coatings. *J. Am. Ceram. Soc.*, 2000, **83**(8), 2023–2028.
7. Subramanian, M. A., Aravamudan, G. and Subba Rao, G. V., Oxide pyrochlores—a review. *Prog. Solid State Chem.*, 1983, **15**, 55–143.
8. Cao, X., Vassen, R., Jungen, W., Schwartz, S., Tietz, F. and Stoever, D., Thermal stability of lanthum zirconate plasma-sprayed coatings. *J. Am. Ceram. Soc.*, 2001, **84**(9), 2086–2090.
9. Dai, H., Zhong, X. H., Li, J. Y., Zhang, Y. F., Meng, J. and Cao, X. Q., Thermal stability of double-ceramic-layer thermal barrier coatings with various coating thickness. *Mater. Sci. Eng. A*, 2006, **433**(1/2), 1–7.
10. Vassen, R., Traeger, F. and Stoever, D., New thermal barrier coatings based on pyrochlore/YSZ double-layer systems. *Int. J. Appl. Ceram. Technol.*, 2004, **1**(4), 351–361.
11. Park, J. G. and Cormack, A. N., Defect energetics and nonstoichiometry in lanthanum magnesium hexaaluminate. *J. Solid State Chem.*, 1997, **130**(2), 199–212.
12. Wang, J. W., Tian, Z. J., Xu, J. G., Xu, Y. P., Xu, Z. S. and Lin, L. W., Preparation of Mn substituted La-hexaaluminate catalysts by using supercritical drying. *Catal. Today*, 2003, **83**(1–4), 213–222.
13. Cao, X. Q., Li, J. Y., Zhang, Y. F., Dai, H., Zhong, X. H. and Meng, J., The preparation and application of catalyst support with high sintering-resistance. Chinese Patent, Appl. no. 200510017298.8.
14. Gadow, R. and Schaefer, G. W., Thermal insulating materials and method for producing SAME. German Patent no. WO 99/42630, 1999.
15. Schaefer, G. W. and Gadow, R., Lanthanum aluminate thermal barrier coating. In *Proceedings of the 23rd Annual International Conference on Composites, Advanced Ceramics, Materials, and Structures*, ed. David E. Clark. Cocoa Beach of Florida, 1999. American Ceramic Society, Westerville, Ohio, USA, 1999, pp. 291–297.
16. Friedrich, C., Gadow, R. and Schimer, T., Lanthanum hexaaluminate—a new material for atmospheric plasma spraying of advanced thermal barrier coatings. *J. Therm. Spray Technol.*, 2001, **10**(4), 592–598.
17. Friedrich, C. J., Gadow, R. and Lischka, M. H., Lanthanum hexaaluminate thermal barrier coatings. In *Proceedings of the 25th Annual International Conference on Composites, Advanced Ceramics, Materials, and Structures: B*, ed. M. Singh and T. Jessen. Cocoa Beach of Florida, January 2001. American Ceramic Society, Westerville, Ohio, USA, 2001, pp. 372–375.
18. Gadow, R. and Lischka, M., Lanthanum hexaaluminate-novel thermal barrier coatings for gas turbine applications-materials and process development. *Surf. Coat. Technol.*, 2002, **151/152**, 392–399.
19. Miller, R. A., Current status of thermal barrier coatings—an overview. *Surf. Coat. Technol.*, 1987, **30**, 1–11.
20. Haynes, J. A., Ferber, M. K. and Porter, W. D., Thermal cycling behavior of plasma-sprayed thermal barrier coatings with various MCrAlY bond coats. *J. Therm. Spray Technol.*, 2000, **38**(9), 38–48.
21. Traeger, F., Ahrens, M., Vassen, R. and Stover, D., A life time model for ceramic thermal barrier coatings. *Mater. Sci. Eng. A*, 2003, **358**(1/2), 255–265.
22. Eldridge, J. I., Spuckler, C. M., Street, K. W. and Markham, J. R., Infrared radiative properties of yttria-stabilized zirconia thermal barrier coatings. In *Proceedings of the 26th Annual International Conference on Advanced Ceramics & Composites*, Cocoa Beach/Cape Canaveral, January 2002, Florida USA, 2002, Paper C8.
23. Cao, X. Q., Application of rare earths in thermal barrier coating materials. *J. Mater. Sci. Technol.*, 2007, **23**(1), 15–35.
24. Gleeson, B., Thermal barrier coatings for aeroengine applications. *J. Propulsion Power*, 2006, **22**(2), 375–383.

25. Padture, N. P., Gell, M. and Jordan, E. H., Thermal barrier coatings for gas-turbine engine applications. *Science*, 2002, **296**, 280–284.
26. Toscano, J., Vassen, R., Gil, A., Subanovic, M., Naumenko, D., Singheiser, L. and Quadakkers, W. J., Parameters affecting TGO growth and adherence on MCrAlY-bond coats for TBC's. *Surf. Coat. Technol.*, 2006, **201**, 3906–3910.
27. Zhang, Y. F., Li, Q., Ma, X. F. and Cao, X. Q., Synthesis and high-pressure sintering of lanthanum magnesium hexaaluminate. *Mater. Lett.*, 2008, **62**, 923–925.
28. Kishitake, K., Era, H. and Baba, S., Tensile strength of plasma-sprayed alumina and/or zirconia coatings on titanium. *J. Therm. Spray Technol.*, 1995, **4**(4), 353–357.
29. Bianchi, L., Denoirjean, A., Fauchais, P. and Postel, O., Generation of alumina plasma sprayed coatings on alumina substrates. In *Thermal Spray: Practical Solutions for Engineering Problems*, ed. C. C. Berndt. ASM International, Materials Park, Ohio, USA, 1996, pp. 749–755.
30. Chraska, P., Dubsky, J., Neufuss, K. and Pisacka, J., Alumina-base plasma-sprayed materials. Part I. phase stability of alumina and alumina-chromia. *J. Therm. Spray Technol.*, 1997, **6**(3), 320–326.
31. Cao, X. Q., Vassen, R., Fisher, W., Tietz, F., Jungen, W. and Stoever, D., Ceramic materials for thermal barrier coatings. *J. Eur. Ceram. Soc.*, 2004, **24**, 1–10.
32. Ozawa, M., Onoe, R. and Kato, H., Formation and decomposition of some rare earth (RE=La, Ce, Pr) hydroxides and oxides by homogeneous precipitation. *J. Alloys Comp.*, 2006, **408–412**, 556–559.
33. Dean, John A., *Lange's Handbook of Chemistry* (*12th ed.*). McGraw-Hill, 1979, pp. 3–120.
34. Brand, P., Troschke, R. and Weigelt, H., Formation of α-Al_2O_3 by thermal decomposition of basic aluminium chlorides at low temperatures. *Cryst. Res. Technol.*, 2006, **24**(7), 671–675.
35. Vassen, R., Kerkhoff, G. and Stoever, D., Development of a micromechanical life prediction model for plasma sprayed thermal barrier coatings. *Mater. Sci. Eng. A*, 2001, **303**, 100–109.